NRIAG JOURNAL OF ASTRONOMY AND GEOPHYSICS
2021, VOL. 10, NO. 1, 168–182
https://doi.org/10.1080/20909977.2021.1902111

ARTICLE

OPEN ACCESS Check for updates

Linear geological structure, traverse orientation and structure resolution and characterisation using 1D and 2D resistivity images

Martins Olusola Olorunfemi[a], Ademakinwa George Oni[a], Taiwo Kazeem Fadare and Odunayo Emmanuel Bamidele[a,b]

[a]Department of Geology, Obafemi Awolowo University, Ile-Ife, Nigeria; [b]Department of Geophysics, Federal University Oye-Ekiti, Oye-Ekiti, Nigeria

ABSTRACT

This paper presents results of previous investigations involving 1D and 2D resistivity imaging of linear geological structures with varying traverse orientations relative to the structure azimuth with a view to determining the effect of such variation on the resolution of the structures. It observed that the orientation of 2D traverse relative to a fault azimuth significantly determines the resolution of the structure while the alignment of 1D vertical electrical sounding (VES) relative to the structure azimuth defines the form of the VES curve and leads to inconsistency in resistivity and thickness estimates and overall depth estimates at deep depth. 2D structures were best resolved with 2D resistivity images when the traverses were established normal (in-line) to the structure azimuth. Structures delineated by in-line 2D images are corroborated by in-line VES interpretation models and confirmed by drillers' logs, whereas the resolution of such structure is impaired on parallel (cross-line) 2D resistivity images/maps with distorted and disjointed image of the investigated fault at deep depth. For two orthogonal VES alignments (in-line and cross-line) to the azimuth of an investigated fault, deviations in layer resistivity values were generally <17% while thickness/depth estimates deviated by as much as 30–78%, at deep depth.

ARTICLE HISTORY
Received 21 April 2020
Revised 25 February 2021
Accepted 8 March 2021

KEYWORDS
Cross-line; in-line; 2D structure; structure azimuth; resolution; ves

1. Introduction

In a simple geological environment with horizontal or near horizontal layering and lateral homogeneity, the vertical electrical sounding (VES) technique of the electrical resistivity method is relevant in subsurface layer delineation and layer thickness or depth to geoelectric interface determination and is, therefore, often applied in engineering site and groundwater investigations in both sedimentary and basement environments (Olorunfemi and Fasuyi 1993; Aina et al. 1996; Edet and Okereke 1997; Ajayi et al. 2005; Olorunfemi et al. 2005; Idornigie et al. 2006; Ojo et al. 2007; Nejad et al. 2011; Shrestha and Shah 2013; Bayowa et al. 2014; Ojo et al. 2015).

However, in a complex geological environment with both lateral and vertical geoelectrical discontinuities, the 1D VES technique (that assumes vertical variations in earth resistivity only) suffers limitation in distorted VES curve (Zohdy et al. 1974) and error in VES data interpretation. In such a complex geological environment, a 2D image of the subsurface is required for the identification of vertical and near-vertical discontinuities such as faults and fractured zones, shear zones, to define basement bedrock topography and identify basement depressions – geological features that are relevant to groundwater accumulation and transmission. This may have informed the growing application of the 2D imaging technique, involving 2D data gathering often with the dipole–dipole array, in groundwater investigation (Chirindja et al. 2017; Gao et al. 2018; Hasan et al. 2018; Olorunfemi and Oni 2019; Olorunfemi et al. 2020). In such cases, the 2D imaging technique is adopted as a reconnaissance technique while the VES is adopted as a confirmatory technique. The integration of the aforementioned geoelectrical survey techniques has significantly improved the success rate of groundwater development through borehole drilling in basement complex environment (Muchingami et al. 2012; Ratnakumari et al. 2012; Kumar et al. 2014; Hasan et al. 2017; Olorunfemi and Oni 2019; Olorunfemi et al. 2020).

However, the earth model is essentially 3D with X, Y and Z axes. 1D earth model that is derived from 1D VES data set is an oversimplification of the earth's model. The VES-derived earth model is a good approximation when the earth model shows resistivity variations in the vertical (Z) only. The deviation from this basic assumption, in practice, accounts for the ambiguities in VES data interpretation. 2D data gathering assumes that the earth resistivity varies in two (X and Z) directions only, that is, laterally and vertically where the lateral variation is along the direction of the

CONTACT Ademakinwa George Oni oniademakinwa@yahoo.com Department of Geology, Obafemi Awolowo University, Ile-Ife, Osun State, Nigeria

traverse line (X direction). Resistivity values are assumed uniform along a direction (Y) perpendicular to the azimuth (direction) of the traverse line. Where such 2D traverse line is established normal to the strike of an inclined geological feature, such as a fault, the 2D technique measures resistivity variations across the dip and with respect to depth while homogeneity (or uniformity) is assumed along the strike of the geological feature, which often time may not be true. This constitutes the basic limitation of the 2D data gathering technique (Loke et al. 2013), in spite of its closeness to defining the 3D earth model, which normally would require two orthogonal 2D images. This paper investigates how the orientation of 2D traverse line and alignment of 1D VES electrode spread relative to the azimuth of investigated linear geological structure affects the resolution of the inverted 2D images of such structure and the determination of its geoelectrical characteristics in a typical basement complex environment.

2. 1D and 2D resistivity data gathering techniques

The 1D VES technique involves measurements of vertical variations in ground resistivity by gradually expanding the current (A, B) and potential (M, N) electrodes (Figure 1(a)) with respect to a fixed centre of the electrode array. The Wenner and the Schlumberger electrode arrays are commonly adopted in the VES technique with the Schlumberger array often preferred due to relative ease of field logistic (two electrodes are moved at a time except when repeated measurements are made) and the adjudged relatively higher depth of investigation with respect to the Wenner array [depth of investigation of 0.125AB

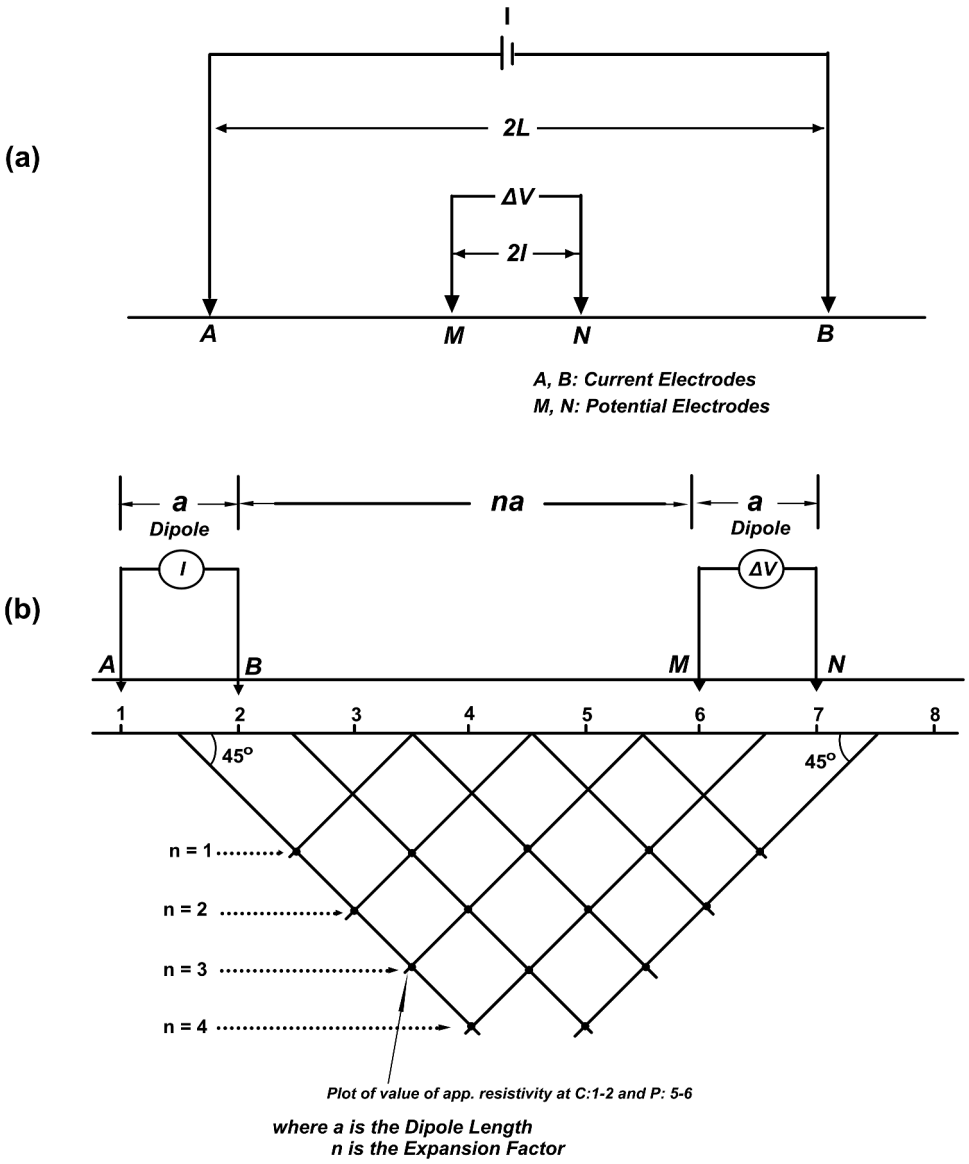

Figure 1. (a) Schlumberger array and (b) dipole–dipole array and data presentation in pseudosection format (culled from Sharma 1997).

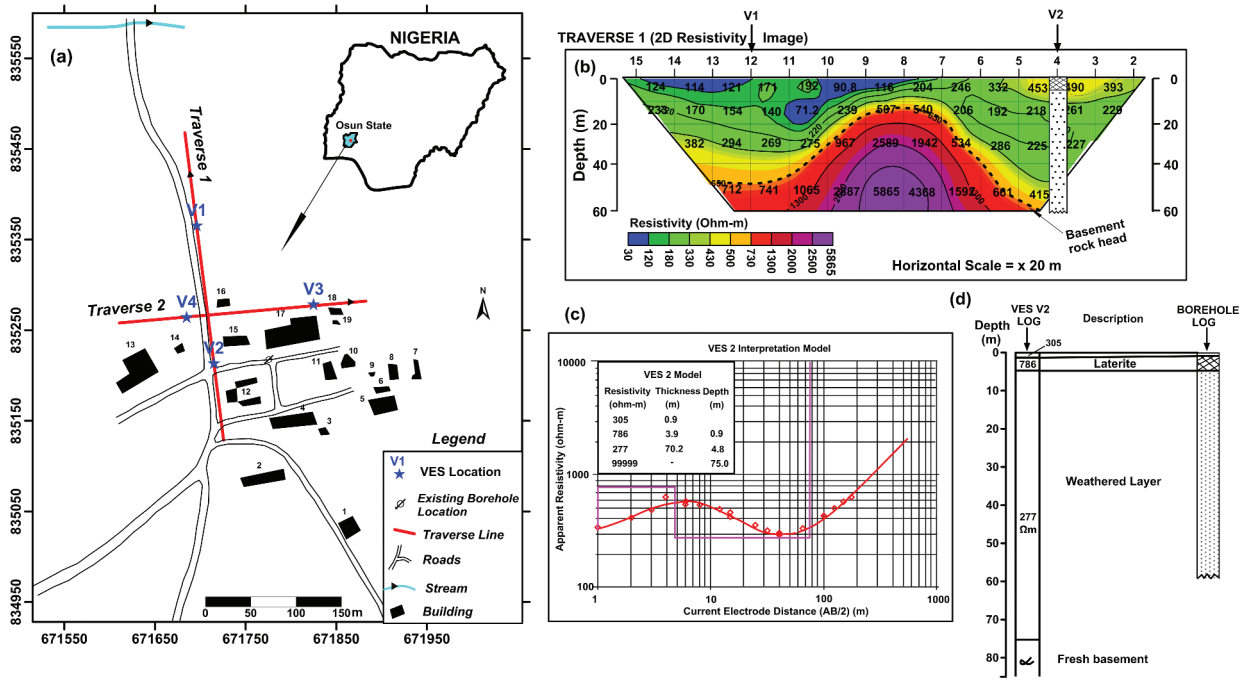

Figure 2. OAU agric farm (site i): (a) location map; (b) 2D image with superimposed VES interpretation model; (c) VES interpretation curve; (d) correlated VES interpretation model and borehole lithological log (culled from Olorunfemi et al. 2018).

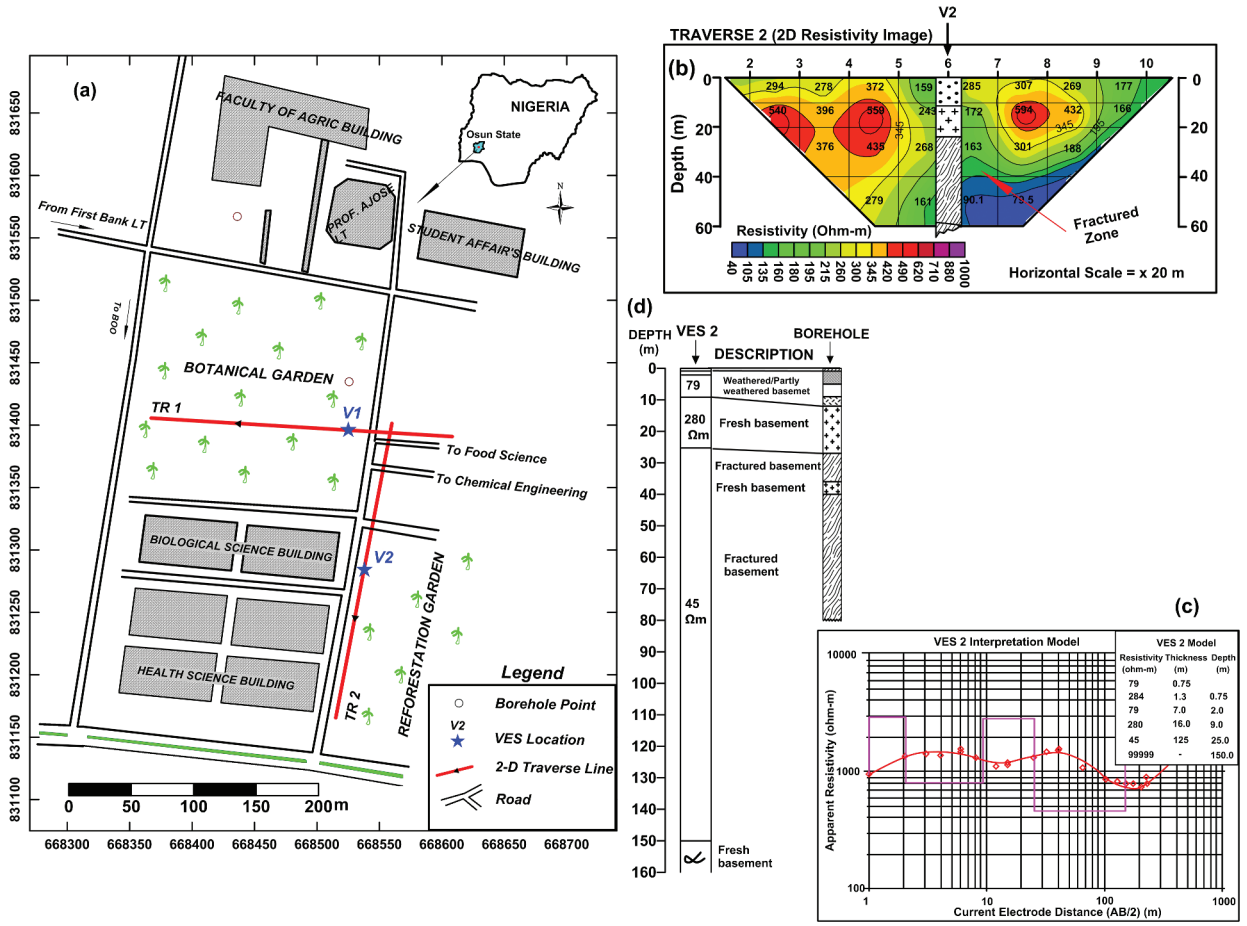

Figure 3. OAU faculty of science (site ii): (a) location map; (b) 2D image with superimposed VES interpretation model; (c) VES interpretation curve; (d) correlated VES interpretation model and borehole lithological log (culled from Olorunfemi et al. 2019).

as against 0.115AB for Wenner array (Roy and Apparao 1971)], where AB is the total current electrode spread length (see Figure 1(a)). The apparent resistivity (ρ_{sc}) equation is defined as

$$\rho_{sc} = \pi R \frac{L^2}{2l} \quad (1)$$

where R ($\Delta V/I$) is ground resistance, L (AB/2) is half current electrode spacing, l (MN/2) is half potential electrode spacing and π is a constant (22/7 or 3.143).

The VES data are presented as VES curves – plots of apparent resistivity against electrode spacings on a bilogarithmic graph paper. For the Schlumberger array, the electrode spacing is AB/2 which is half the current–current electrode spacing (Telford et al. 1990; Reynolds 1997; Keary et al. 2002). The curves are quantitatively interpreted by a method involving partial curve matching and computer-aided 1D forward modelling with software such as W-GeoSoft/WinSev 5.1. The quantitative interpretation of VES curve is not unique. Ambiguities in interpretation are due to equivalence, suppression and dip effect (deviation of geoelectric interface from horizontal). Ambiguities in VES interpretation can be minimised when interpretation is constrained by information from borehole lithological or wireline logs.

2D resistivity data gathering involves a field design that enables measurements of earth resistivity along lateral and vertical directions to be carried out. Several electrode arrays including the dipole–dipole, Wenner, pole–dipole and Wenner–Schlumberger arrays can be adopted. For the dipole–dipole array (Figure 1(b)) that is commonly adopted, the lateral resistivity variations are measured with constant current (A–B) and potential (M–N) dipole spacing (a) and inter dipole (AB–MN) spacing (na) (Figure 1(b)) while the vertical variations are measured with constant current and potential dipole spacing but increasing inter dipole spacing with expansion factor, n, varying from 1 to 5 or even more if deeper depths are of interest (Telford et al. 1990; Reynolds 1997; Keary et al. 2002). The measuring station is the point of intersection of two 45° inclined lines from the midpoints of the current and potential dipoles (Figure 1(b)). The apparent resistivity equation (ρ_{dd}) is defined as

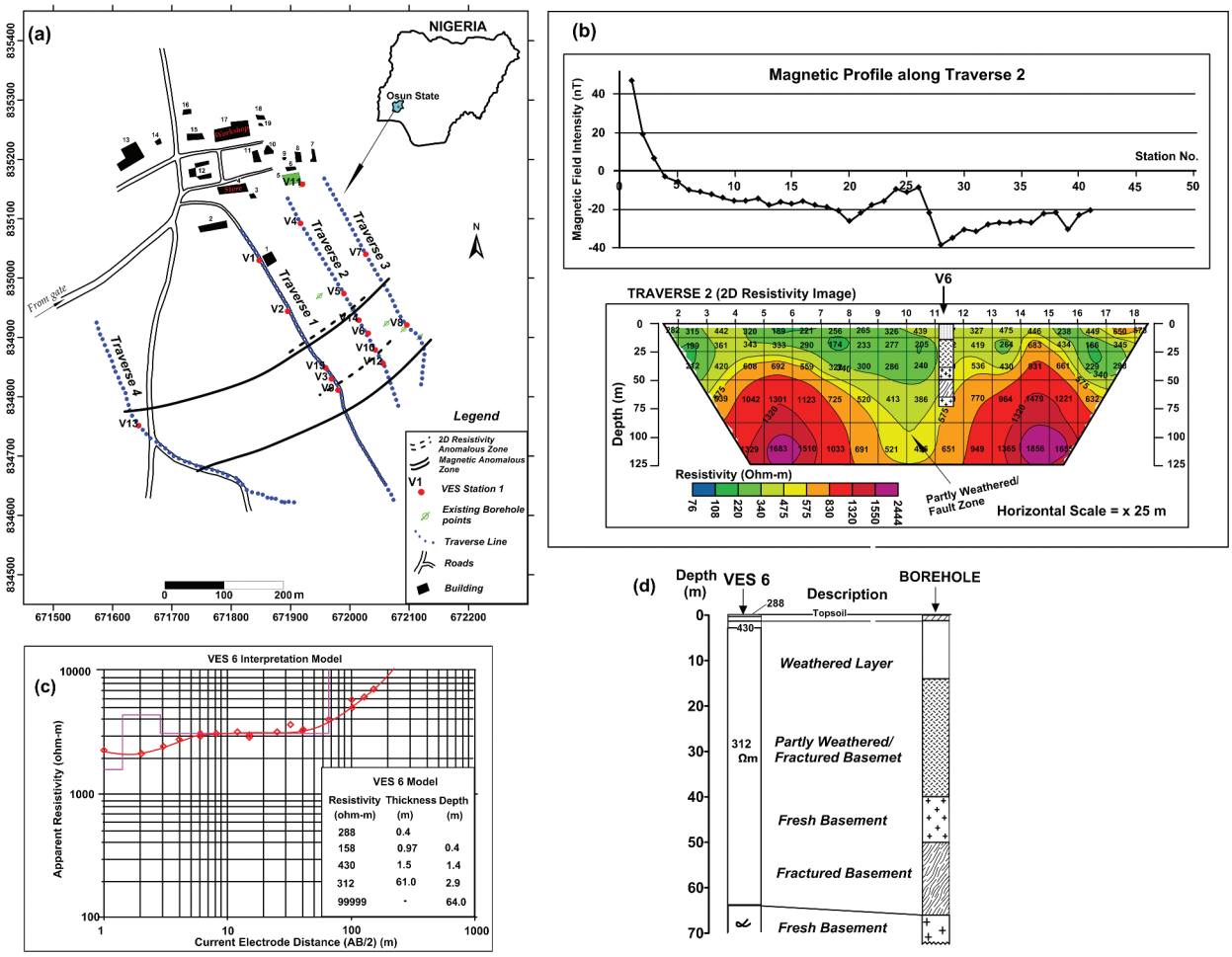

Figure 4. OAU agric farm (site iii): (a) location map; (b) 2D image with superimposed VES interpretation model; (c) VES interpretation curve; (d) correlated VES interpretation model and borehole lithological log (culled from Olorunfemi et al. 2019).

$$\rho_{dd} = \pi aRn(n+1)(n+2) \quad (2)$$

where $R(\Delta V/I)$ is ground resistance, a is the dipole length, n is the expansion factor and π is a constant (22/7 or 3.143).

The quantitative interpretation of 2D resistivity dipole–dipole data involves 2D inversion using appropriate software such as DIPRO for windows. However, inverted images from 2D data could suffer model boundary deformation due to the edge effect (Sumanovac and Dominkovic Alavanja 2007). As in other geophysical methods, the resolution of such images decreases with depth. The advantages of this electrode array include its relatively high depth of investigation, defined as 0.195 AN by Roy and Apparao (1971), where AN is the entire spread length (see Figure 1(b)) at any particular point in time; very high resolution of imaging 2D vertical/or near vertical structures (fault/fractured zones) (Stummer et al. 2004) and the possibility of inverting the 2D data set into real 2D vertical image beneath the traverse line.

3. Assessment of the effectiveness of integrated 1D and 2D resistivity images in groundwater investigation

The 2D electrical imaging technique has, in recent time, found useful applications in groundwater investigation. The inverted 2D resistivity images have been corroborated by 1D VES interpretation models and drillers' borehole logs, as illustrated with few case histories below. In all the case histories, W-GeoSoft/WinSev 5.1 and DIPRO for Windows software were, respectively, used for the forward modelling of 1D VES and inversion of 2D dipole–dipole resistivity data.

3.1. Case history I

2D dipole–dipole imaging was used as a reconnaissance technique to define the basement bedrock topography and hence the overburden thickness in an area underlain by mica schist within the

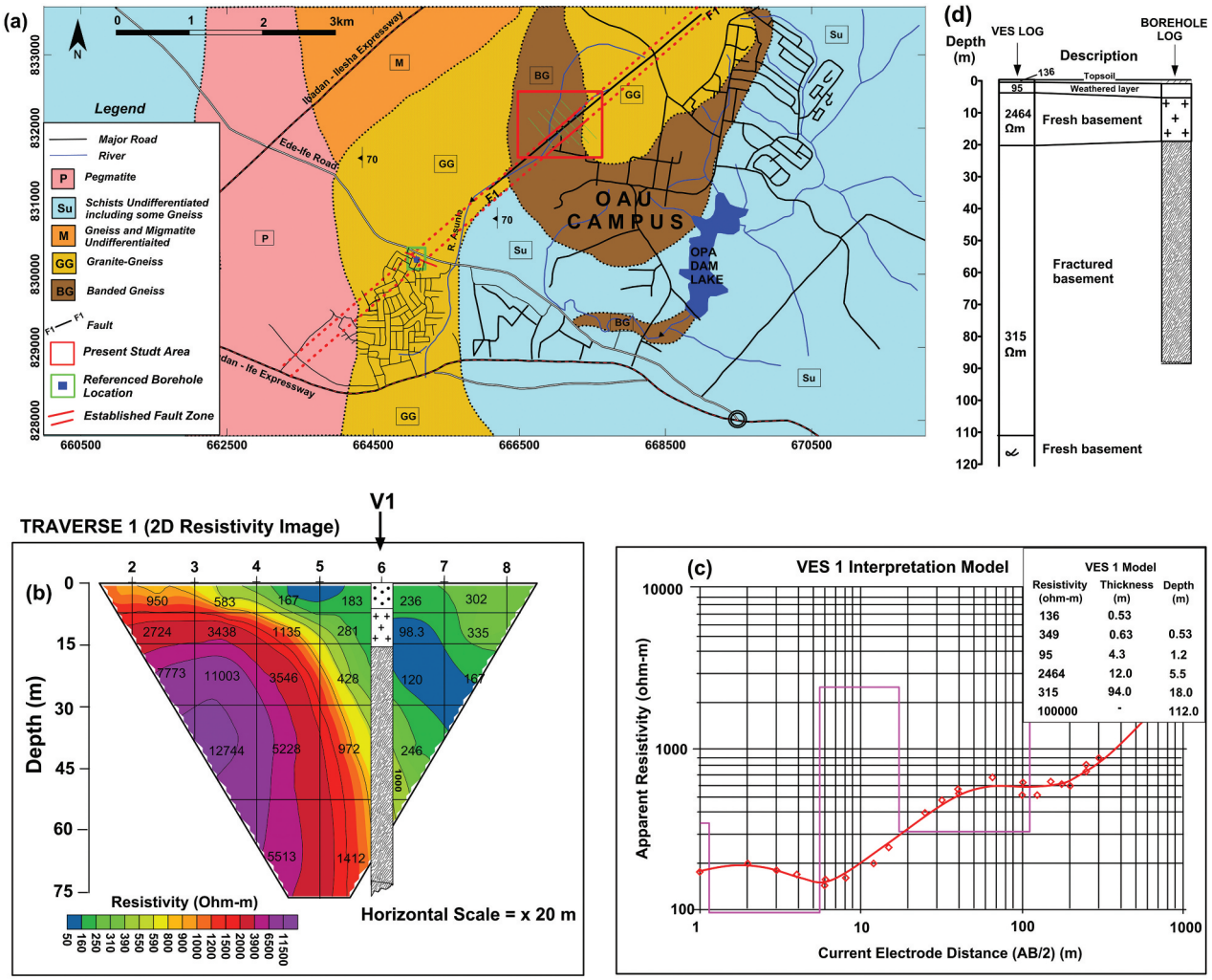

Figure 5. Modomo Ile-Ife (site iv): (a) geological/location map; (b) 2D image with superimposed VES interpretation model; (c) VES interpretation curve; (d) correlated VES interpretation model and borehole lithological log (modified from Olorunfemi et al. 2020).

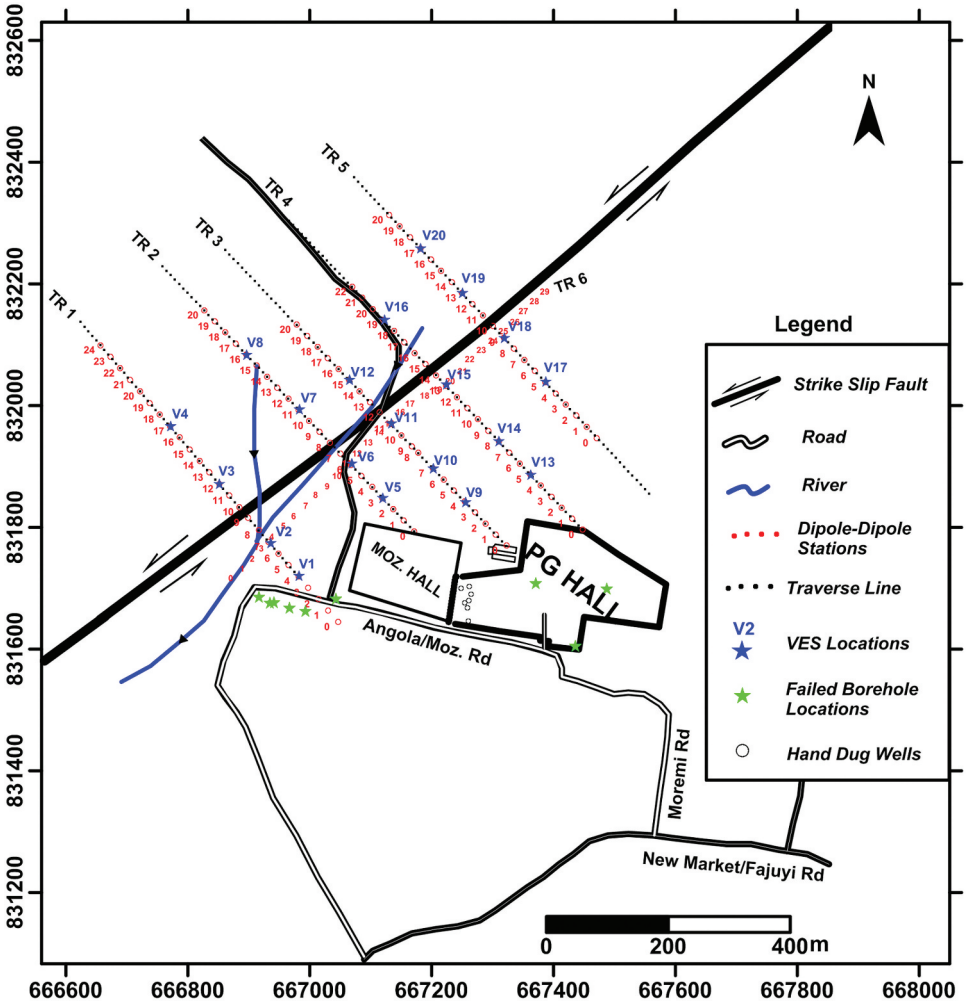

Figure 6. Geophysical data acquisition map showing 2D in-line (TR 1–5) and cross-line (TR 6) resistivity traverses and the vertical electrical sounding locations (modified after Olorunfemi et al. 2020).

estate of Obafemi Awolowo University (OAU), Ile-Ife, Nigeria (Olorunfemi et al. 2018). Follow-up and confirmatory 1D VES (V1 and V2) corroborated the 2D resistivity images. The drilled site (VES station 2) is located within an area with a thick weathered layer, which was confirmed by drilling (see Figure 2). The borehole was terminated at a depth of 60 m within the weathered basement. The lithological log correlates perfectly well with the VES interpretation model and the 2D image. The borehole is productive with groundwater yield of 1.3 l/s.

3.2. Case history II

2D dipole–dipole resistivity imaging technique was employed to map fractured basement in an area underlain by near-surface grey gneiss within OAU Ile-Ife, Nigeria, using the characteristics of low-resistivity vertical discontinuity within a high-resistivity fresh basement host rock (Olorunfemi and Oni 2019). Confirmatory VES was carried out to investigate the characteristics of the 2D structure which was identified to be a fractured basement column. This was corroborated by the driller's log (Figure 3). The borehole was terminated within the VES-delineated fractured basement with a groundwater yield of 1.5 l/s. The 2D image, VES interpretation model and driller log show perfect correlation.

3.3. Case history III

2D dipole–dipole resistivity imaging technique was carried out across a prominent low (negative) total field magnetic anomaly characteristic of a fault zone within a schistose basement bedrock (Olorunfemi and Oni 2019). The suspected fault zone manifests on the 2D image as a low-resistivity discontinuity within high-resistivity fresh basement host rock. The structure was confirmed with a VES as a fractured basement column and subsequently drilled with a groundwater yield of 2.2 l/s. The 2D image, VES interpretation model and the borehole lithological log show perfect correlation (Figure 4).

3.4. Case history IV

2D dipole–dipole resistivity imaging technique was used to identify fractured basement zone as a low-resistivity vertical discontinuity within a high-

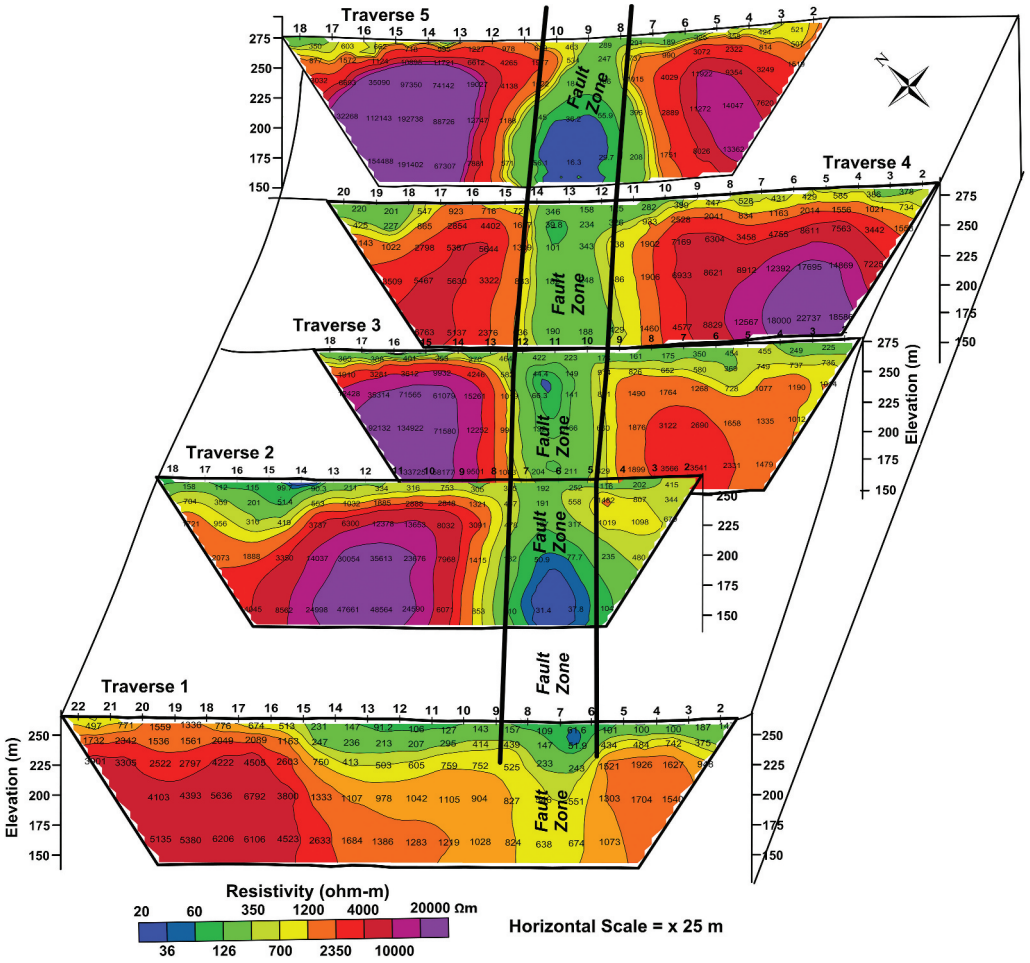

Figure 7. Correlated 2D images across in-line traverses (modified after Olorunfemi et al. 2020).

resistivity fresh granite gneiss basement host rock (Olorunfemi et al. 2020). The structure was confirmed using the VES technique, and the VES station was subsequently drilled with a groundwater yield of 2.0 l/s. The borehole was terminated within the VES-established fracture basement column. The 2D image, VES interpretation model and the borehole lithological log show perfect correlation (Figure 5).

4. Investigating the effect of 2D traverse orientation relative to the azimuth of structure

The case histories outlined above demonstrate the effectiveness and reliability of 2D images in groundwater investigation. But for the requirement of information on borehole depth and details of the subsurface sequence, borehole could be sited directly with the 2D images.

In case histories III and IV, the orientations of the 2D image traverses were approximately normal to the azimuth of the suspected structure. Geological structure is best imaged when geophysical traverses are established normal to its trend. In other case histories, the geological features (basement depression and fractured basement column) that were picked were assumed to be delineated by traverses at a high angle to the structure trend, otherwise the image resolution would have been poor.

In a recent geophysical investigation for groundwater development in a basement complex area with generally low groundwater potential (Olorunfemi et al. 2020), a remote sensing established regional strike–slip fault was investigated using integrated magnetic profiling and resistivity 1D and 2D imaging techniques. Five in-line traverses (TR1–5) established approximately normal to the fault were occupied (Figure 6). In addition, a sixth cross-line traverse (TR 6) was established along the centre of the established fault zone (Figure 6). The aim was to use the sixth traverse to investigate if a cross-line (2D traverse line) will image the fault zone with the same resolution as displayed by the correlated five earlier in-line traverses established across the structure.

4.1. 2D images acquired along in-line traverses normal to the azimuth of investigated strike–slip fault

The correlated 2D resistivity structures (images) (Figure 7 and 2D) geoelectric sections (Figure 8)

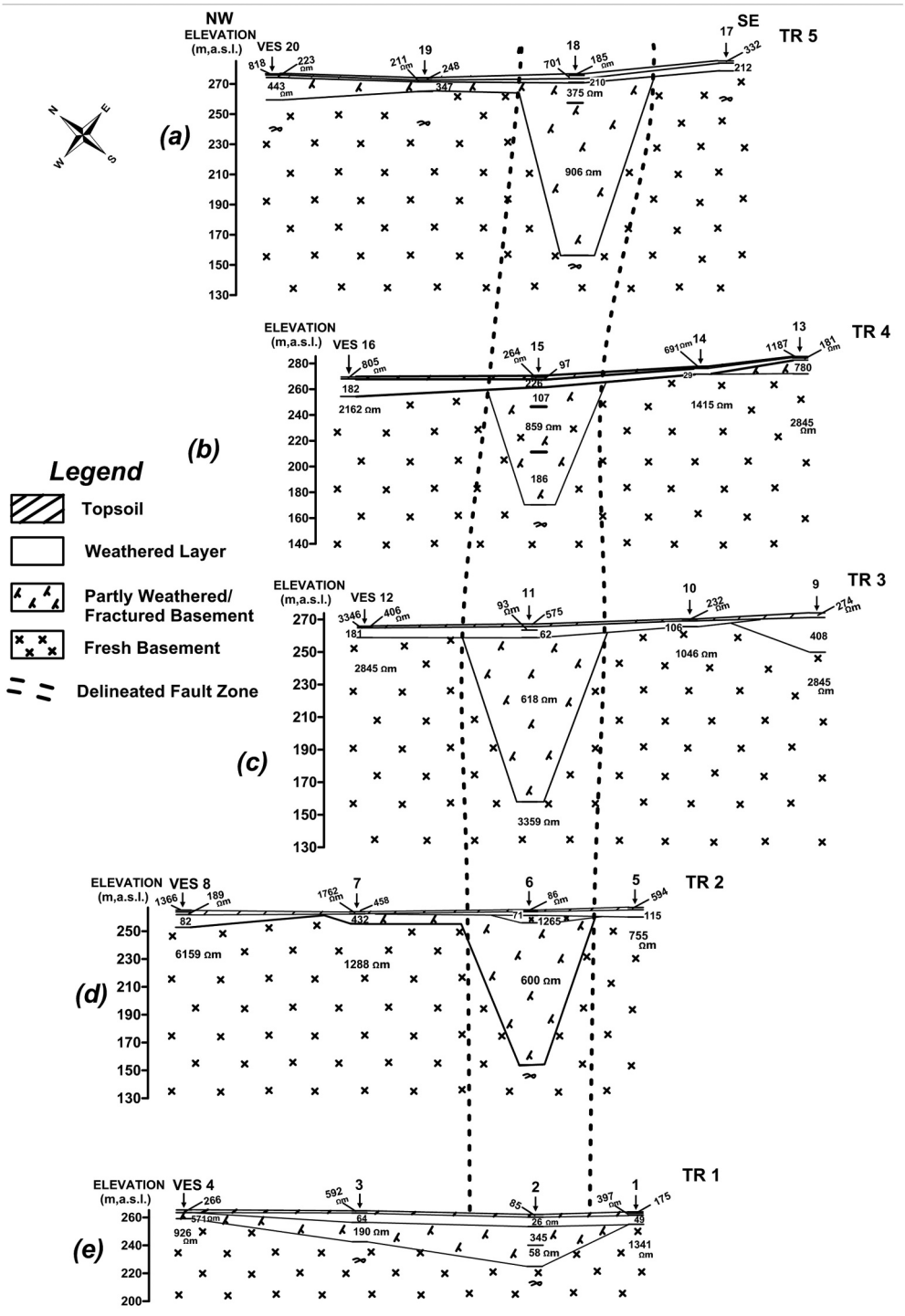

Figure 8. Correlated geoelectric sections across in-line traverses TR 1–5 (culled from Olorunfemi et al. 2020).

across the traverses identify a fault zone about 112–150 m wide with depth extent in excess of 150 m (Olorunfemi et al. 2020) as relatively low-resistivity vertical discontinuity within a high-resistivity fresh basement host rock (Figure 8) within the remote sensing geo-referenced fault line that coincides with the northwestern edge of the delineated fault zone (Figure 9). In plan, the resistivity depth slice maps generated from the 2D images also established the fault zone as a relatively linear low-resistivity zone which becomes more pronounced at deep depth >50 m and whose depth extent goes beyond 125 m (Figure 10). The geo-referenced strike–slip fault trace also coincides with the northwestern edge of the linear low resistivity.

4.2. Cross-line 2D image parallel to the azimuth (strike direction) of the strike–slip fault

Figure 11 shows the 2D resistivity image obtained along a traverse parallel to the azimuth of the delineated fault zone. VES 2B, 6B, 11B, 15B and 18B are cross-line VES whose direction of electrode expansion is aligned parallel to the azimuth of fault which occupy

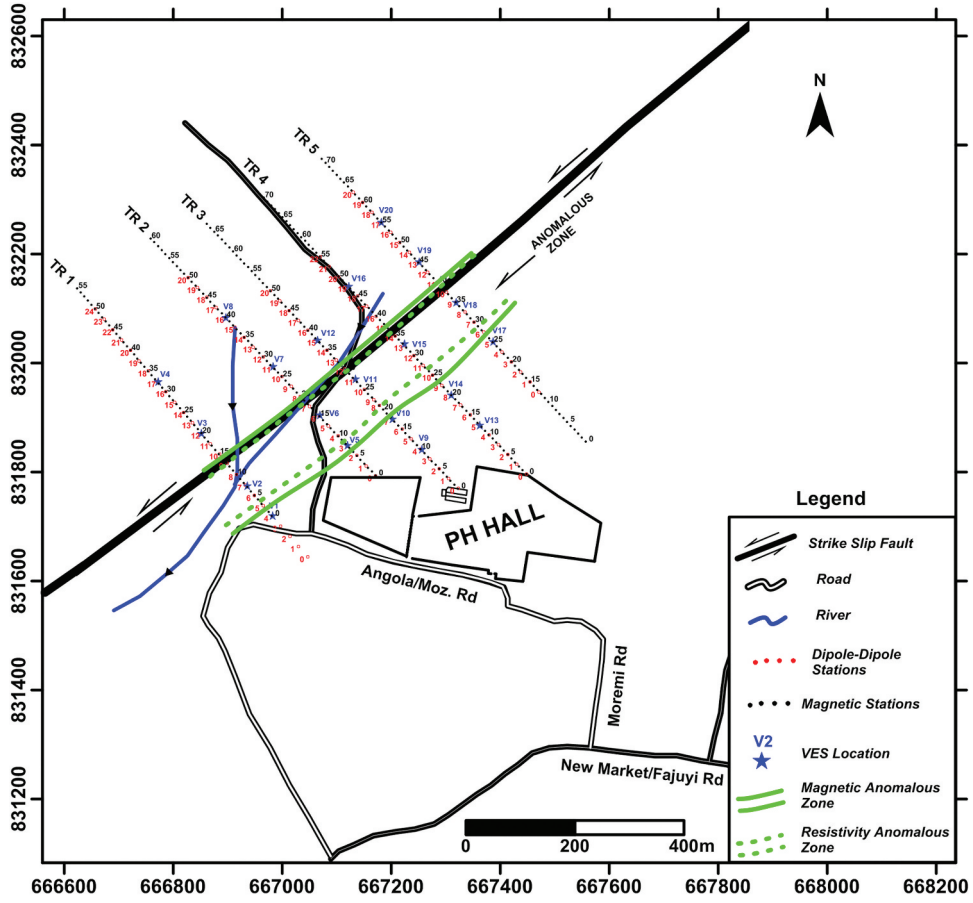

Figure 9. Structure map showing correlated magnetic and resistivity anomalous zones (culled from Olorunfemi et al. 2020).

corresponding locations of in-line VES 2, 6, 11, 15 and 18 whose direction of electrode expansion is aligned perpendicular to strike of fault. The VES stations were located at centres of low-resistivity vertical discontinuities interpreted to be indicative of a fault zone (Figure 7). Contrary to the image of a fault zone with a significant depth extent (in excess of 150 m) exhibited by the in-line 2D images, Figure 11 presents an image of a near-surface intrusion-like basement rock beneath VES 2/2B, 6/6B, 11/11B and 15/15B and a basement depression beneath VES18/18B. The image identifies a vertical discontinuity suspected to be another fault zone between VES 2/2B and 6/6B. This could be a cross fault to the established major strike–slip fault.

Figure 12(a–e) displays the depth slice resistivity maps generated from combined in-line and cross-line 2D images. At depth ranges of up to 25–50 m, the depth slice maps (Figure 12(a–c)) are not significantly different from depth slice map generated from in-line 2D images (Figure 10(a–c)) with the geo-referenced fault trace constituting the northwestern edge of patches of linearly oriented relatively low-resistivity zone. At deeper depths (>25–50 m and up to 87.5–125 m) the in-line depth slice maps (Figure 10 (d, e)) show more diagnostic characteristic features of the fault in continuous low-resistivity zone as against the disjointed and discontinuous patches of low-resistivity images of the combined in-line and cross-line depth slice maps (Figure 12(d, e)). This distortion arose from the poor resolution of the cross-line 2D image at deep depth.

Figure 13(a, b) compares the 2D geoeletric sections generated from the in-line and cross-line VES, respectively, along the centre of the investigated fault zone. Table 1 compares the geoelectric parameters of the two geoelectric sections. Both sections identify four subsurface layers composed of the topsoil, weathered layer, partly weathered/fractured basement and fresh basement bedrock. The partly weathered/fractured basement column characterised the fault zone. The referenced table shows deviations in estimates of resistivities and thicknesses of the subsurface layers: 3–65% (but generally <10%) and 8–62% (but generally <42%) for the topsoil; 3–7% and 9–23% (but generally <15%) for the weathered layer; 4–44% (but generally <17%) and 37–78% for partly weathered/fractured basement; 30–74% deviation in depth to rock head for a uniformly generally very resistive basement. The relatively large variation ranges in the estimated resistivties and thicknesses of the topsoil are due to the varying heterogeneous (anisotropic) nature of the topsoil. With the exception of the topsoil, deviation in resistivity estimates obtained from the in-line and cross-line VES is generally less than 20% and hence

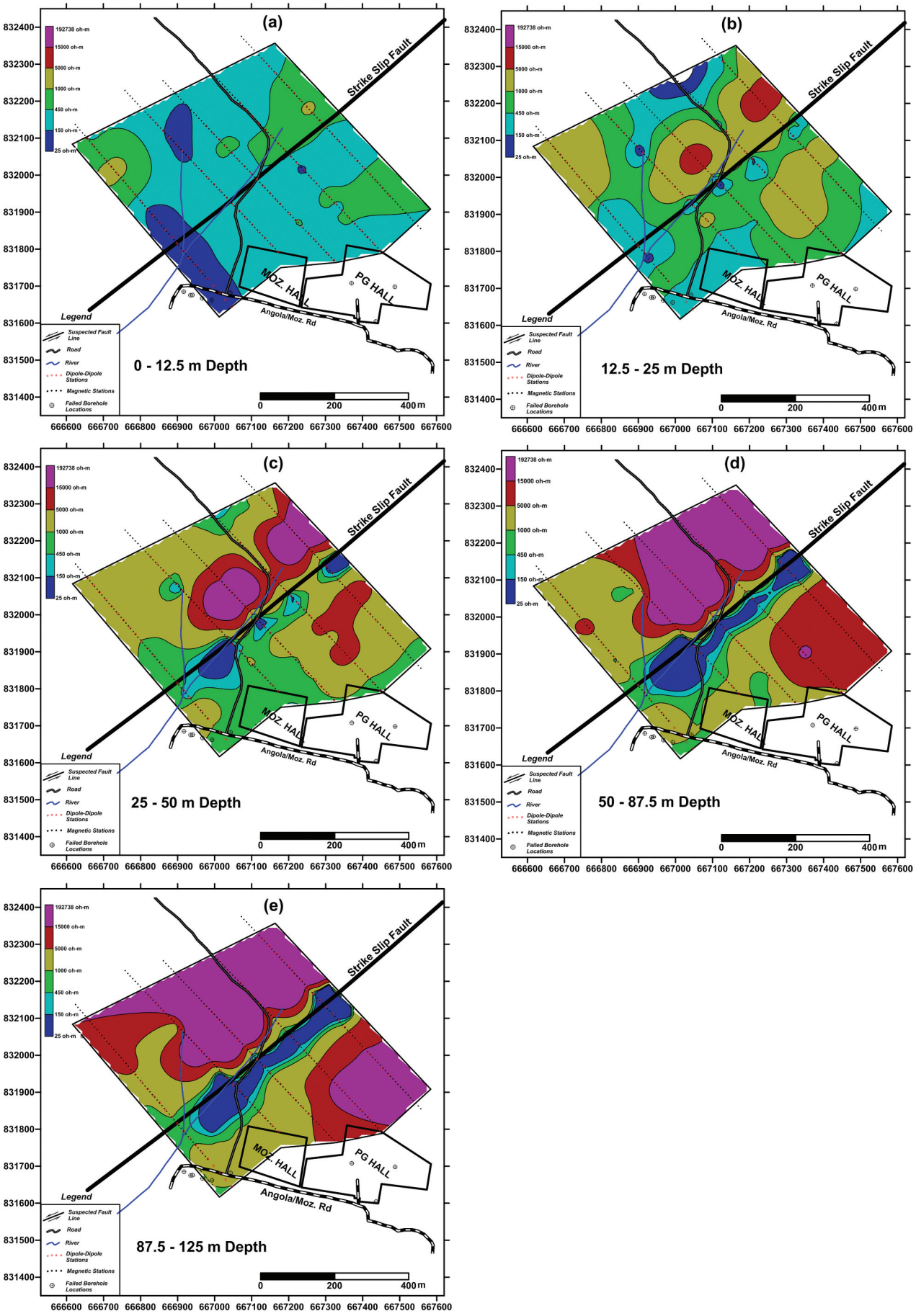

Figure 10. Resistivity depth slice maps at (a) 0–12.5 m, (b) 12.5–25 m, (c) 25–50 m, (d) 50–87.5 m and (e) 87.5–125 m depth levels generated from in-line traverses (culled from Olorunfemi et al. 2020).

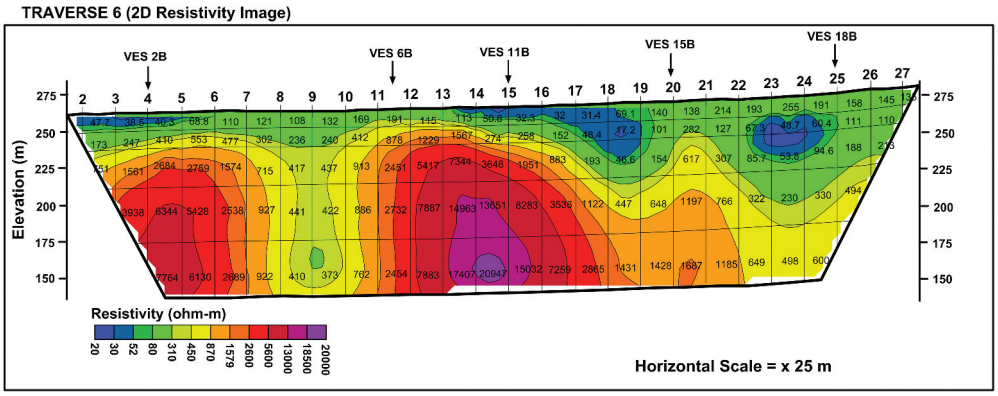

Figure 11. 2D resistivity structure along cross-line traverse TR 6.

within the limits of interpretation error. Deviations in estimates of thickness at shallow depth (<10 m) are also generally <15%. This is also reflected in the similarity of the two geoelectric sections at shallow depth (see Figure 13(a, b)). Figure 13(b) (which mirrors Figure 11), however, shows that the significantly thick partly weathered/fractured column in the in-line geoelectric section was grossly underestimated by as much as 37–78%, while the depth to basement bedrock was underestimated by 30–74% by the cross-line geoelectric section.

5. Discussion

This study assumes a geological model of a homogeneous low-resistivity water-saturated fault block with infinite strike length but finite depth extent hosted by a more resistive fresh basement host rock. However, variations in the degree of weathering and fracturing and in the degree of fluid saturation, in addition to varying depth extent of the fault zone, as currently established, will create inhomogeneity within the fault zone. The contrast in resistivity between the fault zone and the host rock is required for its delineation. In essence, therefore, to resolve such a structure, geophysical traverses must be established normal (or at a high angle) to the structure for 2D imaging. This may explain the poor characterisation of the fault zone by a cross-line 2D image (Figure 11). As observed by Olorunfemi and Opadokun (1987, 1989) electrical anisotropy in the basement complex environment, due to inhomogeneity arising from geological structures such as dykes, faults, joints and foliation planes, could lead to errors (deviations) in estimates of geoelectric parameters (layer resistivities of up to 90%) and thicknesses or depths (of up to 68%).

Figure 14(a–e) shows the superimposed plots of the in-line (normal alignment) and cross-line (parallel alignment to the azimuth of fault) for the five VES points located along the middle of the fault zone (Figure 6). The superimposed VES curves show significant overlap at short electrode spacings of up to 6–12 m for most of the VES stations after which the curves are separated, though with significant retention in form. The overlap of both VES curves at small electrode spacings accounts for the significant agreement in both layer resistivity and thickness estimates at shallow depth. The cross-line VES curves slightly differ in form on the rising segment of the VES curves due to the suppression of the confined fractured basement which characterised the fault zone as reflected in the cross-line 2D image (Figure 11). The inflections which characterised basement fractures on the rising segments of the VES curves (Olorunfemi and Fasuyi 1993; Ojo and Olorunfemi 2013) are missing (suppressed) or poorly defined on the cross-line VES curves. This makes the cross-line VES curves to rise at higher gradients (Figure 14(a–e)) than the in-line curves at large electrode spacings. The similarity in form of the VES curves makes deviations in interpreted layer resistivity values small while suppression of the fractured basement column led to underestimation of depths to the fresh basement rock head, as earlier observed. For the two orthogonal VES alignments [normal (in-line) and parallel (cross-line)] to the azimuth of the investigated fault, deviations in layer resistivity values were generally < 17% while thickness/depth estimates deviated by as much as 30–78%, at deep depth.

6. Conclusion

The orientation of 2D traverse relative to the azimuth (strike direction) of a fault trace significantly determines the resolution of the 2D image while the alignment (i.e. direction of expansion of electrodes) of 1D VES relative to the structure azimuth defines the form of the VES curve and leads to inconsistency (errors) in resistivity and thickness estimates and the overall depth estimates at deep depth. 2D structures are best resolved with 2D resistivity images when the 2D

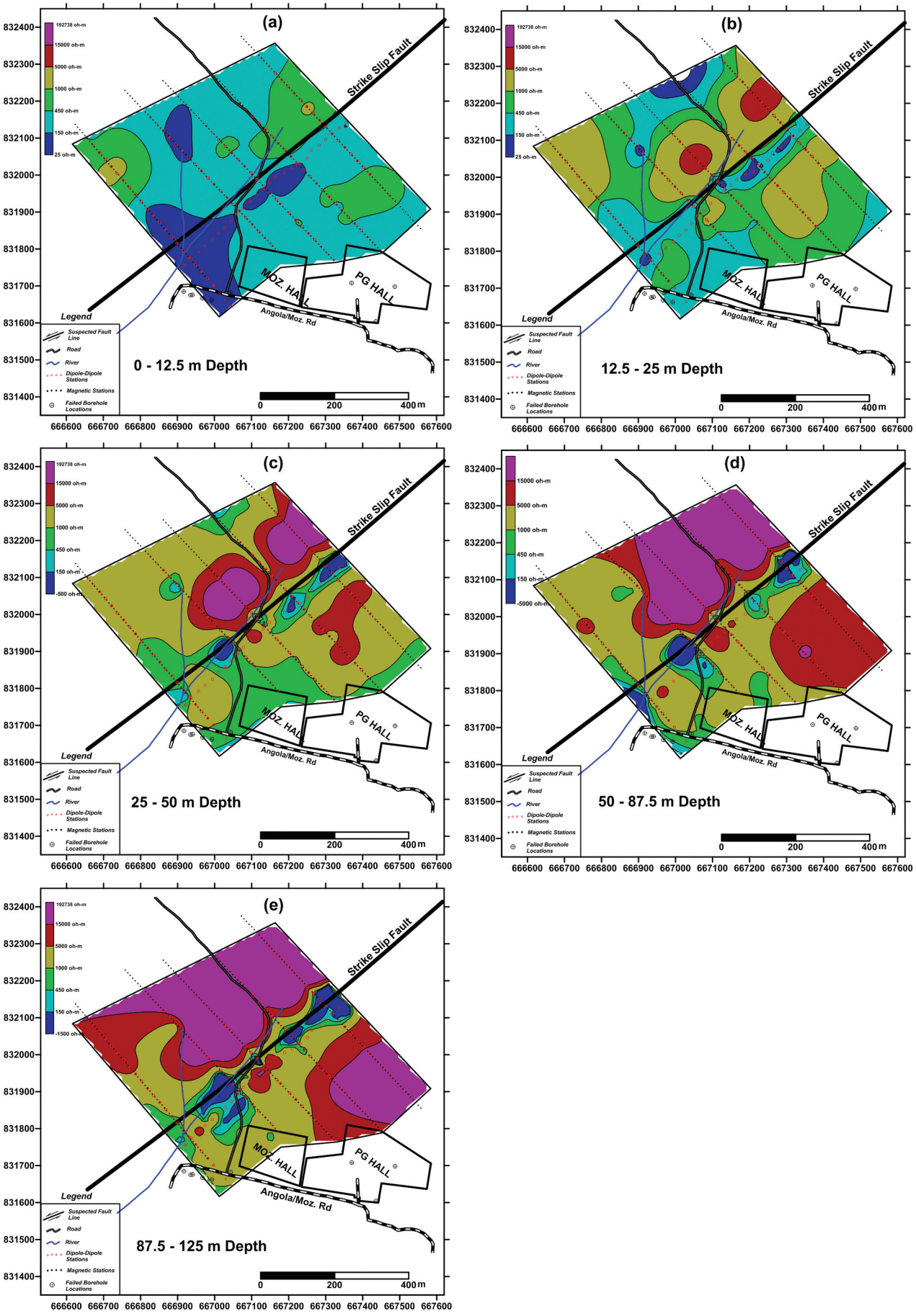

Figure 12. Resistivity depth slice map at (a) 0–12.5 m, (b) 12.5–25 m, (c) 25–50 m, (d) 50–87.5 m and (e) 87.5–125 m depth levels generated from combined in-line and cross-line traverses.

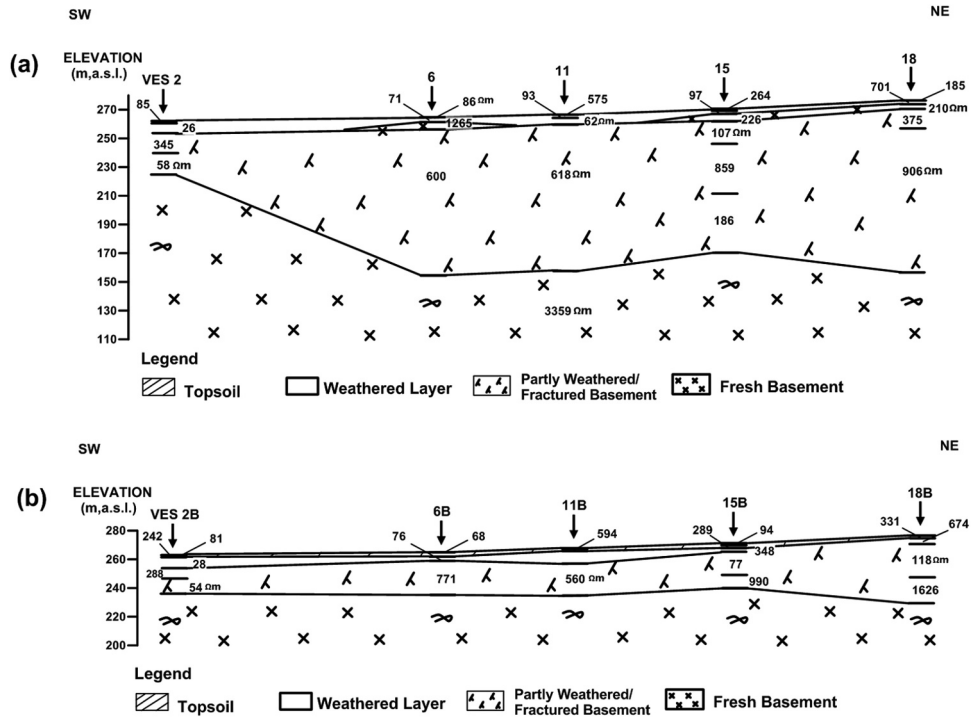

Figure 13. Geoelectric sections connecting (a) in-line VES stations 2, 6, 11, 15 and 18 and (b) cross-line VES stations 2B, 6B, 11B, 15B and 18B along the centre of the 2D resistivity images delineated fault zone.

Table 1. Comparison of in-line and cross-line VES interpreted geoelectrical parameters

VES No	INTERPRETED GEOELECTRIC PARAMETERS							
	Topsoil		Weathered Layer		Partly Weathered/Fractured Basement		Fresh Basement bedrock	
	Resistivity (Ωm)	Thickness (m)	Resistivity (Ωm)	Thickness (m)	Resistivity (Ωm)	Thickness (m)	Resistivity (Ωm)	Depth to Rock Head (m)
2	85	1.9	26	6.2	345/58	28.3	∞	37
2B	81/242	1.1	28	7.1	288/54	17.8	∞	26
6	86	0.8	71	2.6	600	102.2	∞	110
6B	68	1.9	76	3.2	771	23.9	∞	29
11	579	1.2	93/62	6.7	618	101.1	3358	109
11B	594	1.3	65	8.7	560	22.9	∞	32
15	264	1.0	97	1.5	226/107/859 /186	97.5	∞	100
15B	289	0.9	94	1.3	348/77/990	27.8	∞	30
18	185	0.6	-	-	701/210/375 /906	119.4	∞	120
18B	331	1.6	-	-	674/118/1620	45.4	∞	47
Deviation (in %)	3-65% but generally <10%	8-62% but generally <42%	3-7%	9-23% but generally <15%	4-44% but generally <17%	37-78%	Generally unaffected	30-74%

traverses are established at a high angle (normal) to the azimuth.

The case histories presented in this paper demonstrate that structures delineated by in-line 2D images are corroborated by in-line VES interpretation models and confirmed by drillers' logs, whereas the resolution of such structure is impaired when 2D traverses are established parallel (cross-line) to or at a low angle to the azimuth of the structure, as shown in the distorted and disjointed image of the investigated fault at deep depth, in the cross-line 2D resistivity structure and the combined in-line and cross-line depth slice maps, respectively. For the two orthogonal VES alignment [normal (in-line) and parallel (cross-line)] to the azimuth of an investigated fault, deviations in layer resistivity values were generally <17% while thickness/depth estimates deviated by as much as 30–78%, at deep depth.

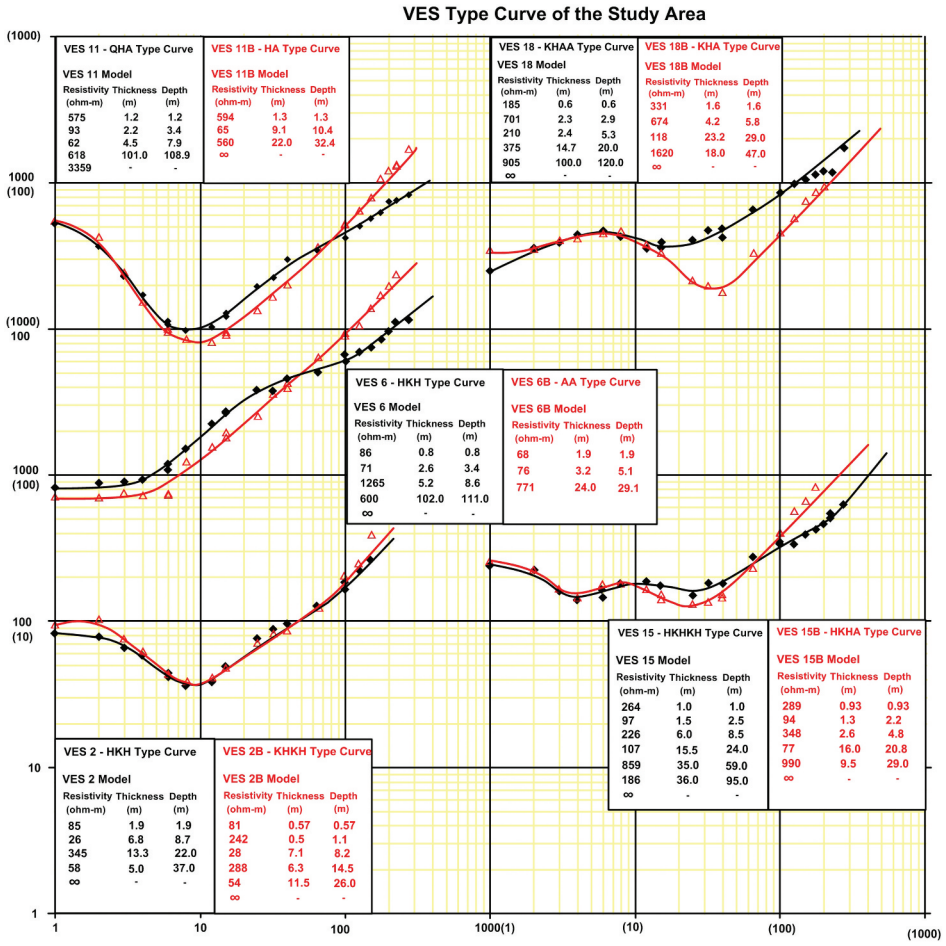

Figure 14. Superimposed in-line (black line) and cross-line (red line) VES curves obtained along the centre of the fault zone.

Disclosure statement

The authors declare that there is no conflict of interest

ORCID

Martins Olusola Olorunfemi http://orcid.org/0000-0003-3494-3333
Ademakinwa George Oni http://orcid.org/0000-0003-0627-7820

References

Aina A, Olorunfemi MO, Ojo JS. 1996. An integration of aeromagnetic and electrical resistivity methods in dam site investigation. Geophys. 61(2):349–356.

Ajayi O, Olorunfemi MO, Ojo JS, Adegoke-Anthony CW, Chikwendu KK, Oladapo MI, Idornigie AI, Akinluyi F. 2005. Integrated geophysical and geotechnical investigation of a damsite on river Mayo Ini, Adamawa State, northern Nigeria. Afr Geosci Rev. 12(3):179–188.

Bayowa GO, Olorunfemi MO, Ademilua OL. 2014. A geoelectric assessment and classification of the aquifer systems in a typical basement complex terrain; case study of Ekiti State, southwestern Nigeria. Res J Eng & Appl Sci. 3(1):55–60.

Chirindja J, Dahlin T, Juizo D. 2017. Improving the groundwater well siting approach in consolidated rock in Nampula province, Mozambique. Hydrogeo J. 25 (5):1423–1435. doi:10.1007/s10040-017-1540-1.

Edet AE, Okereke CS. 1997. Assessment of hydrogeological conditions in basement aquifers of the Precambrian Oban Massif, southeastern Nigeria. J A Geophy. 36(4):195–204. doi:10.1016/S0926-9851(96)00049-3.

Gao Q, Shang Y, Hasan M, Jin W, Yang P. 2018. Evaluation of a weathered rock aquifer using ERT methods in South Guangdong, China. Water. 10(3):293. doi:10.3390/w10030293.

Hasan M, Shang Y, Akhter G, Jin W. 2017. Geophysical assessment of groundwater potential: a case study from Mian Channu area, Pakistan. Groundwater. doi:10.1111/gwat.12617

Hasan M, Shang Y, Jin W. 2018. Delineation of weathered/fracture zones for aquifer potential using an integrated geophysical approach: a case study from South China. J A Geophys. 157:47–60. doi:10.1016/j.jappgeo.2018.06.017.

Idornigie AI, Olorunfemi MO, Omitogun AA. 2006. Electrical resistivity determination of subsurface layers, subsoil competence and soil corrosivity at an engineering site location in Akungba-Akoko, southwestern Nigeria. IJS. 8(2):139–177.

Keary P, Brooks M, Hill I. 2002. An introduction to geophysical exploration. Third ed. UK: Blackwell Science Ltd., Oxford.

Kumar D, Rao VA, Sarma VS. 2014. Hydrogeological and geophysical study for deeper groundwater resource in quartzitic hard rock ridge region from 2D resistivity data. J Earth Syst Sci. 123(3):531–543. doi:10.1007/s12040.014-0408-1.

Loke MH, Chambers JE, Rucker DF, Kuras O, Wilkinson PB. 2013. Recent developments in the direct-current geoelectrical imaging method. J Appl Geophys. 95:135–156. doi:10.1016/j.jappgeo.2013.02.017

Muchingami I, Hlatywayo DJ, Neil JM, Chuma C. 2012. Electrical resistivity survey for groundwater investigation and shallow subsurface evaluation of the basaltic greenstone formation of the urban Bulawayo aquifer. Phys Chem Earth. 50-52:44–51. doi:10.1016/j.pce.2012.08.014.

Nejad HT, Mumipour M, Kaboli R, Najib OA. 2011. Vertical electrical sounding (VES) resistivity survey technique to explore groundwater in an arid region, southeast Iran. J Appl Sci. 11(23):3765–3774. doi:10.3923/jas.2011.3765.3774.

Ojo AO, Olorunfemi MO. 2013. Resistivity modeling of confined fractured basement column for varying thicknesses and depth of burial. The Pacific J Sci & Tech. 14 (1):464–475.

Ojo JS, Olorunfemi MO, Akintorinwa OJ, Bayode SO, Go O, Fo A. 2015. GIS integrated geomorphological, geological and geoelectrical assessment of the groundwater potential of Akure metropolis, southwest Nigeria. J Earth Sci & Geotech Eng. 5(14):85–101.

Ojo JS, Olorunfemi MO, Omosuyi GO. 2007. Geoelectric sounding to delineate shallow aquifers in the coastal plain sands of Okitipupa area. S W Nigeria Online J Earth Sci. 1 (4):170–179.

Olorunfemi MO, Adekola SA, Oni AG, Adewale E, Fadare TK, Ehinola P, Bamigboye M 2018 Geophysical survey for groundwater development within the premises of the teaching and research farm, Obafemi Awolowo university, Ile-Ife, Osun State. Technical Report, pp18.

Olorunfemi MO, Fasuyi SA. 1993. Aquifer types and the geoelectric/hydrogeologic characteristics of part of the central basement terrain of Nigeria (Niger State). J Afr Earth Sci. 16(3):309–317. doi:10.1016/0899-5362(93)90051-Q.

Olorunfemi MO, Fatoba JO, Ademilua LO. 2005. Integrated VLF-electromagnetic and resistivity survey for groundwater in a crystalline basement complex terrain of southwest Nigeria. Global J Geol Sci. 3(1):71–80.

Olorunfemi MO, Oni AG. 2019. Integrated geophysical methods and techniques for sitting productive boreholes in basement complex terrain of southwestern Nigeria. IJS. 21(1):013–026.

Olorunfemi MO, Oni AG, Bamidele OE, Fadare TK, Aniko OO. 2020. Combined geophysical investigations of the characteristics of a regional fault zone for groundwater development in a basement complex terrain of south-west Nigeria. SN Applied Sciences (Springer Nature Journal). 6. doi:10.1007//s42452-020-2363-6.

Olorunfemi MO, Opadokun MA. 1987. On the application of surface geophysical measurement in geological mapping- the basement complex of southwestern Nigeria as a case study. J Afr Earth Sci. 6(3):287–291.

Olorunfemi MO, Opadokun MA. 1989. Electrical anisotropy in a basement complex area and its effect on depth sounding interpretation results. Nigerian J Mining & Geol. 25(1&2):87–95.

Ratnakumari Y, Rai SN, Thiagarajan S, Kumar D. 2012. 2D electrical resistivity imaging for delineation of deeper aquifers in a part of the Chandrabhaga river basin, Nagpar District, Maharastra. India Curr Sci. 102 (1):62–69.

Reynolds JM. 1997. An introduction to applied and environmental geophysics. England: John Wiley and Sons Ltd.

Roy A, Apparao A. 1971. Depth of investigation in direct current methods. Geophys. 36(5):943–959. doi:10.1190/1.1440226.

Sharma PV. 1997. Environmental and engineering geophysics. Cambridge: Cambridge University Press. p. 475.

Shrestha SR, Shah S 2013 Vertical electrical sounding (VES) survey in Kaski District (Lrkhnath Municipality, Kaski), India. Technical Report, Government of Nepal, Ministry of Irrigation, Groundwater Resources Development Board, Babarmahal (Kathmandu, India), pp37.

Stummer P, Maurer H, Green A. 2004. Experimental design: electrical resistivity data sets that provides optimum subsurface information. Geophys. 69(1):120–139. doi:10.1190/1.1649381.

Sumanovac F, Dominkovic Alavanja S. 2007. Determination of resolution limits of electrical tomography on the block model in a homogeneous environment by means of electrical modeling. Rudarsko-geolosko-naftni Zbornik. 19:47–56.

Telford WM, Gedart LP, Sheriff RE. 1990. Applied geophysics (second edition). Cambridge: Cambridge University Press.

Zohdy AAR, Eaton GP, Marbey DR. 1974. Application of surface geophysics to groundwater investigations: in techniques of water resources investigations of the United States geological survey, book 2. Chapter. D1:22–25.